IEEE Access
Multidisciplinary | Rapid Review | Open Access Journal

Received October 17, 2016, accepted November 29, 2016, date of publication December 7, 2016, date of current version January 4, 2017.

Digital Object Identifier 10.1109/ACCESS.2016.2636341

Research on Design Method and Electromagnetic Vibration of Six-Phase Fractional-Slot Concentrated-Winding PM Motor Suitable for Ship Propulsion

MINGZHONG QIAO, CHAO JIANG, YONGXIN ZHU, AND GENG LI
College of Electrical Engineering, Naval University of Engineering, Wuhan 430033, China

Corresponding author: M. Qiao (qiaomingzhong@126.com)

This work was supported by the National Science Foundation of China under Project 51277177 and Project 51007094.

ABSTRACT In the background of high-power propulsion application on ships and existing uncertain electromagnetic and vibration features of multiphase fractional-slot concentrated-winding permanent magnet (PM) motor, the electromagnetic design and analysis methods of six-phase fractional-slot concentrated-winding PM motor are presented. Four different pole and slot combination schemes are sifted out, and air-gap magnetic field and electromagnetic force of these four motors are studied in contrast. On the basis of the above, a 20-kW prototype of six-phase fractional-slot concentrated-winding PM motor with 48 slots and 44 poles is designed and manufactured, and its electromagnetic and vibration performances are tested through experiments. The test results are in good agreement with calculations, which could guide the development of high-power ship propulsion.

INDEX TERMS Fractional-slot, concentrated-winding, modal analysis, electromagnetic vibration, six-phase PM motor.

I. INTRODUCTION

With development of control theory and power electronics used in AC motor, multi-phase motor with fractional slot and concentrated winding have remarkable advantages in power density and end length of winding [1], [2]. This kind of motor can be adequate for new warships as it could meet with the requirements in low speed and limited installation space, which the ships pose to the high-power propulsion motors. But, odd and even harmonics of MMF exist in such motors [3]. When q(slots per pole per phase) is improperly selected, hidden trouble of vibration will be brought out, which is very dangerous to high-power propulsion motor in warships.

It is well understood that, electromagnetic vibration caused by the electromagnetic force is the main source of motor vibration and noise [4]. Problems related to fractional-slot motor have been widely discussed around the world. Alberti discussed how different teeth-slot combination and winding layer influenced the torque ripple and losses [5]; Rukmi optimized a fractional-slot concentrated-winding motor with 18 slots and 14 poles, which had a large speed-adjusting and low torque-ripple capability [6]. Van analyzed the influence of radial electromagnetic force harmonics on motor vibration of three kind of three-phase PM motors with 12 slots 8 poles, 24 slots 8 poles and 12 slots 10 poles, and concluded that lower step radial forces contributed more in vibration [4]. The radial and tangential torque on teeth of five different three-phase PM motors, whose slot-pole combination are respectively 18/6, 9/6, 12/8, 15/10 and 12/10 were studied in [7], and the noise intensity of different slot-pole combination were also calculated. Lee discussed the no-load and load vibration force of 3 phase fractional-slot concentrated-winding BLDC motor with various slot-pole combination, concluding that the vibration force would reach to its maximum when the slot-pole combination is 12/10 [8]. Vibration and noise of concentrated-winding motor with 12 slots 8 poles and 12 slots 10 poles were analyzed in [9]. Lei studied the influence of permanent magnet size and slot type on vibration of a three-phase fractional-slot concentrated-winding PM motor [10]. The researches above are of much value, but they mainly focus on low-power and 3 phase motors instead of multi-phase high-power low-speed PM motors applied to ships. So it is necessary to proceed in relevant research.

This paper aims at the six-phase fractional-slot concentrated-winding PM motor, which is suitable for low-speed and high-power propulsion on ships. The restraint conditions of slot-pole combination are obtained, and four design schemes in background of high-power and low-speed application are given. A prototype is designed, and experiment results are in good agreement with the theory, indicating the validity of method and design proposed in this paper. This will provide guidance for the high-power design and analysis of this kind of motor.

II. DESIGN OF SIX-PHASE FRACTIONAL-SLOT CONCENTRATED-WINDING PM PROPULSION MOTOR

A. RESTRAINT CONDITIONS OF SIX-PHASE SEMI-SYMMETRIC FRACTIONAL-SLOT CONCENTRATED WINDING

In the six-phase semi-symmetric winding, two three-phase windings apart from each other 30° electrical angle (in the six-phase symmetric winding, two three-phase windings apart from each other 60° electrical angle). According to the law from star graph of slot potential, the angle between two adjacent vectors in star graph should be aliquot by 30, so that two three-phase windings can apart from each other 30° electrical angle, namely:

$$\frac{30}{\left(360/Z_0\right)} = Integer \tag{1}$$

In equation (1), Z_0 is the number of slots in the unit machine.

As a result, available slot number should be integral times of 12.

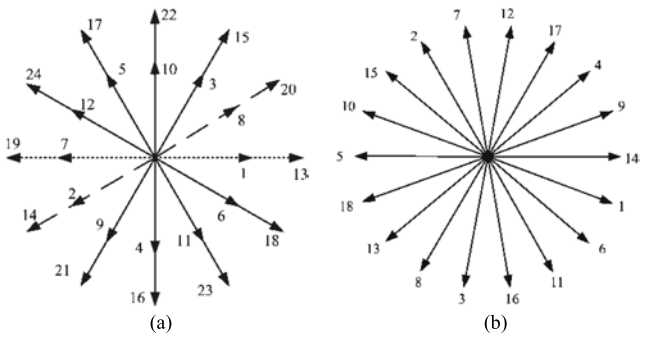

FIGURE 1. The vector star graph comparison while Z/2t is even or odd. (a) Z/2t is even. (b) Z/2t is odd.

Considering that star graph of slot potential consists of spokes (the number of spoke is Z/t) and each spoke contains some vectors (the number of vectors is t), the result of Z/2t should be even, so that the odd and even vectors in the opposite direction can correspond to each other. As shown in Fig.1 (a), the unit machine number, represented by t, in the 24-slot 20-pole motor is2, and its star graph contains 12 spokes, each of which includes 2 same vectors. The dotted and segmented lines indicate slot potential vectors of phase A1 and A2 respectively. Some vector numbers such as 19, 7, 1 and 13 (odd) are in opposite directions, and vector numbers such as 14, 2, 8 and 20 (even) are located in two adjacent spokes. As to the case that spoke number is odd times of 2, Fig.1 (b) is star graph of slot potential of a 18-slot 14-pole motor, and the vector number in its positive and negative spoke are odd and even respectively. In this situation, six-phase semi-symmetric winding cannot be achieved.

Through induction we find that double layer winding can be achieved if Z/2t is even, and either double or single layer winding can be achieved if Z/4t is even. This finding is helpful in designing the motor.

TABLE 1. Six-phase half-symmetrical fractional-slot concentrated-winding Z/P combination selection.

Z/p	12	24	36	48	60
1					
2					
3					
4					
5	*12/5(D)*				
6					
7	*12/7(D)*				
8					
9					
10		24/10(D)			
11		*24/11*			
12					
13		*24/13*	*36/13(D)*		
14		24/14(D)			
15			36/15 (D)		
16					
17			*36/17(D)*	*48/17*	
18					
19			*36/19(D)*	*48/19*	
20				48/20(D)	
21			36/21(D)		
22				48/22	
23			*36/23(D)*	*48/23*	*60/23(D)*
24					
25				*48/25*	60/25(D)
26				48/26	

The available combination schemes are listed in Table I. The cell labeled by numbers can realize the six-phase semi-symmetric fractional-slot concentrated-winding motor. The unit machine groups are marked in italic font. In addition, the cell including "D" means the winding of this combination can only be realized in double layers.

TABLE 2. Basic parameters of the motors with different slot-pole combination.

Slot-pole combination	Core length (mm)	Thickness of PM(mm)	Conductors per slot	Imax(A)
48/44	245	10	34	24
48/46	245	10	34	24
48/50	245	10	34	24
48/52	245	10	34	24

B. DESIGN SCHEME OF LOW-SPEED PROPULSION MOTOR USED IN WARSHIP

Schemes feasible in designing and manufacturing can be obtained by sifting the restraint conditions of six-phase fractional-slot concentrated-winding motor mentioned above. The schemes synthesize the requirements in high power, low speed (0∼300r/min), inverter characteristic, control algorithm and axial size of motor. In order to promote further study of influences from different slot-pole combination on electromagnetic vibration, four design schemes of six-phase fractional-slot concentrated-winding motor are proposed, with slot-pole combination including 48/44, 48/46, 48/50 and 48/52. These four motors are all PM motor with the same power (20kW) and structure parameters, just as shown in Table II. They are all surface magnet motors with open type stator slot and should also meet the conditions as follows:

1) Fundamental magnetic field produced by stator should be same;

2) Fundamental magnetic field produced by rotor should be same; no-load fundamental wave of EMF should be same;

3) Average value of electromagnetic torque at rated current should be same.

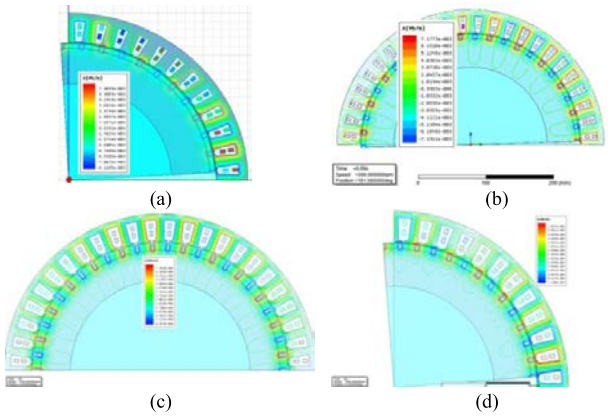

FIGURE 2. No load magnetic flux line of motors. (a) 48 slots/ 44 poles. (b) 48 slots/ 46 poles. (c) 48 slots/ 50 poles. (d) 48 slots/ 52 poles.

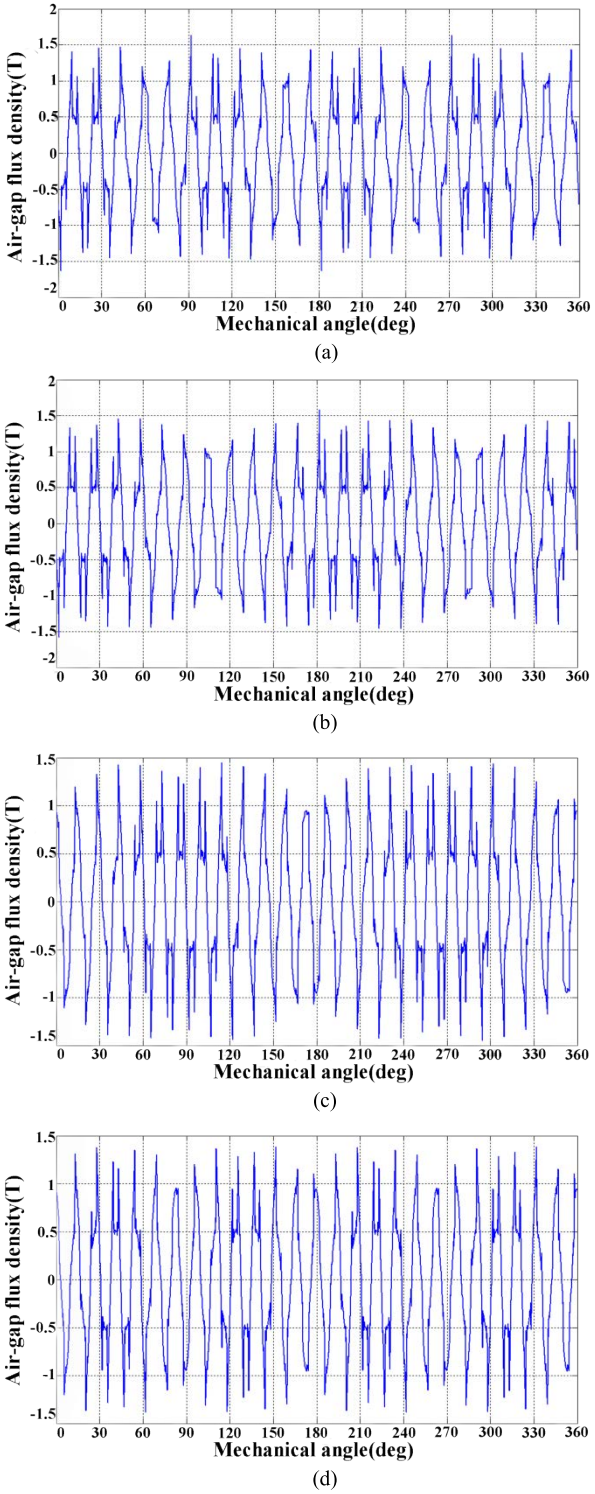

FIGURE 3. No load air-gap flux of motors. (a) 48 slots/ 44 poles. (b) 48 slots/ 46 poles. (c) 48 slots/ 50 poles. (d) 48 slots/ 52 poles.

III. COMPARISION AND ANALYSIS OF ELECTROMAGNETIC CHARACTERISTIC OF DIFFERENT MOTOR SCHEMES

Fig.2 shows the structure and no-load magnetic field distribution of four motors. Fig.3 describes magnetic flux density distribution at no load of four motors, and Table III shows the harmonic components of flux density in Fig.3. For motor with 44 poles, its main wave (order 22) is nearly 0.9T, while other components are quite little.

Fig.4 is the magnetic flux density harmonic distribution at rated load of four motors, and the harmonic components of

TABLE 3. Comparison of vibration of motor with different slot-pole combination.

Slot-pole combination	Radial force order and average value in a time period(KN/m^2)	Distribution of air-gap flux density on rated load	Distribution of air-gap flux density on no load(at some moment)
Case 1: 48 slots 44 poles	4order：15.865 44order：151.7 (main wave) 48order：95.67 52order：38.74 92order：67.93 96order：74.26	22degree：0.8798 T (main wave) 23degree：2% 26degree：10.45% 70degree：23.278% 74degree：11.82%	22degree：0.8985T (main wave) 23degree：2.17% 26degree：11.19% 70degree：22.78% 74degree：11.9%
Case 2: 48 slots 46 poles	2order：18.8278 46order：148 (main wave) 48order：94.58 50order：37.66 94order：67.5 96order：71.76	22degree：2.47% 23degree：0.874 T (main wave) 25degree：10.68% 71degree：23.69% 73degree：11.37%	22degree：2.47% 23degree：0.889T (main wave) 25degree：10.95% 71degree：23.81% 73degree：11.42%
Case 3: 48 slots 50 poles	2order：16.85 46order：36.8 48order：91.75 50order：141.87 (main wave) 96order：70.15 98order：66.8	25degree：0.8642 T (main wave) 23degree：9.1% 26degree：2.42% 71degree：12% 73degree：24%	25degree：0.8731T (main wave) 23degree：9.3% 26degree：2.4% 71degree：12.2% 73degree：24.3%
Case 4: 48 slots 52 poles	4order：19.8 44order：36.55 48order：89.58 52order：139.24 (main wave) 96order：71.03 100order：66.31	26degree：0.8558 T (main wave) 22degree：9.34% 25degree：2.63% 70degree：11.8% 73degree：2.02% 74degree：24%	22degree：10.07% 25degree：2.62% 26degree：0.8755T (main wave) 27degree：2.62% 70degree：11.99% 74degree：22.98%

flux in Fig.4 is shown in Table III. For motor with 44 poles, its main wave (order 22) is nearly 0.88T, while other components are quite little.

IV. COMPARISION AND ANALYSIS OF VIBRATION CHARACTERISTIC OF DIFFERENT MOTOR SCHEMES

According to Maxwell law, radial electromagnetic force suffered by motor can be expressed as follow:

$$F_r = \frac{1}{2\mu}(B_r^2 - B_t^2) \tag{2}$$

In equation (2), Fr is radial Maxwell electromagnetic force; μ is air permeability; Br and Bt are radial and tangential flux density respectively.

In equation (3), the effect of frame is ignored, and the stator is simplified into single ring type. Only yoke deformation of stator core is considered, and the teeth and winding are regarded as additional mass. As a result, the static deformation of stator core caused by radial electromagnetic force can be expressed as:

$$d_s = \frac{3}{4}\frac{F_r}{E}\left(\frac{D_e}{h_e}\right)^3 \frac{l}{\gamma^3} \times 10^6 \tag{3}$$

In the equation above, Fr is radial electromagnetic force; E is elastic modulus; D_e is average diameter of stator yoke; h_e is height of stator yoke; γ is order of force ($\gamma > 0$).

When the order of radial electromagnetic force is 0, the static deformation of stator core caused by radial electromagnetic force can be expressed as:

$$d_s = \frac{F_r}{E}\frac{D_e}{h_e} \times 10^6 \tag{4}$$

Under the 0 order force, the stator conducts uniform radial vibration, and its natural frequency can be expressed as:

$$f_{\gamma 0} = \frac{1}{\pi D_e}\sqrt{\frac{E}{\rho_i \Delta_0}} \tag{5}$$

In equation (5), ρ_i is density of stator core; Δ_0 is addition core coefficient of mass under the 0 order force, $\Delta_0 = 1 + \frac{G_t + G_w}{G_e}$; G_t, G_w, G_e are mass of stator teeth, winding and yoke respectively.

When the force order is 1, vibration happens to the core as it is affected by unilateral magnetic force. The natural frequency of this kind of vibration is:

$$f_{\gamma 1} = f_{\gamma 0}\sqrt{\frac{2}{1 + \frac{1}{\sqrt{3}}\frac{h_e \Delta_\gamma}{\Delta_0 D_e}}} \tag{6}$$

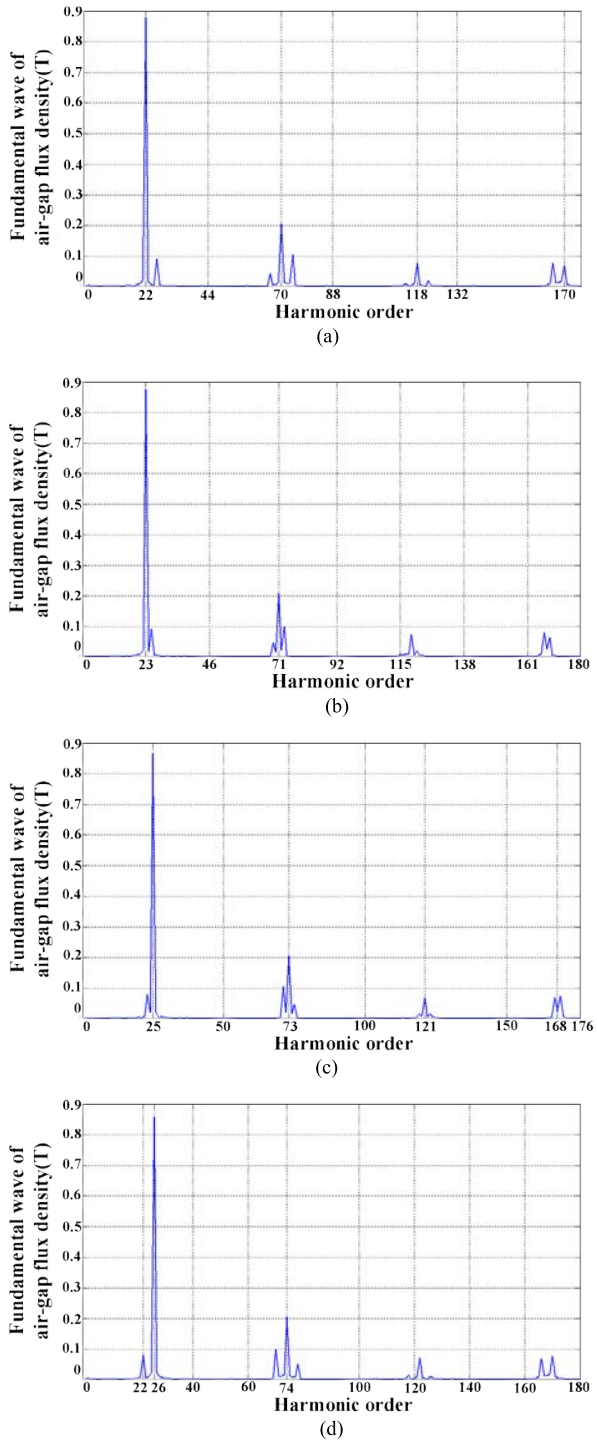

FIGURE 4. Rated load air-gap flux density harmonic distribution. (a) 48 slots/ 44 poles. (b) 48 slots/ 46 poles. (c) 48 slots/ 50 poles. (d) 48 slots/ 52 poles.

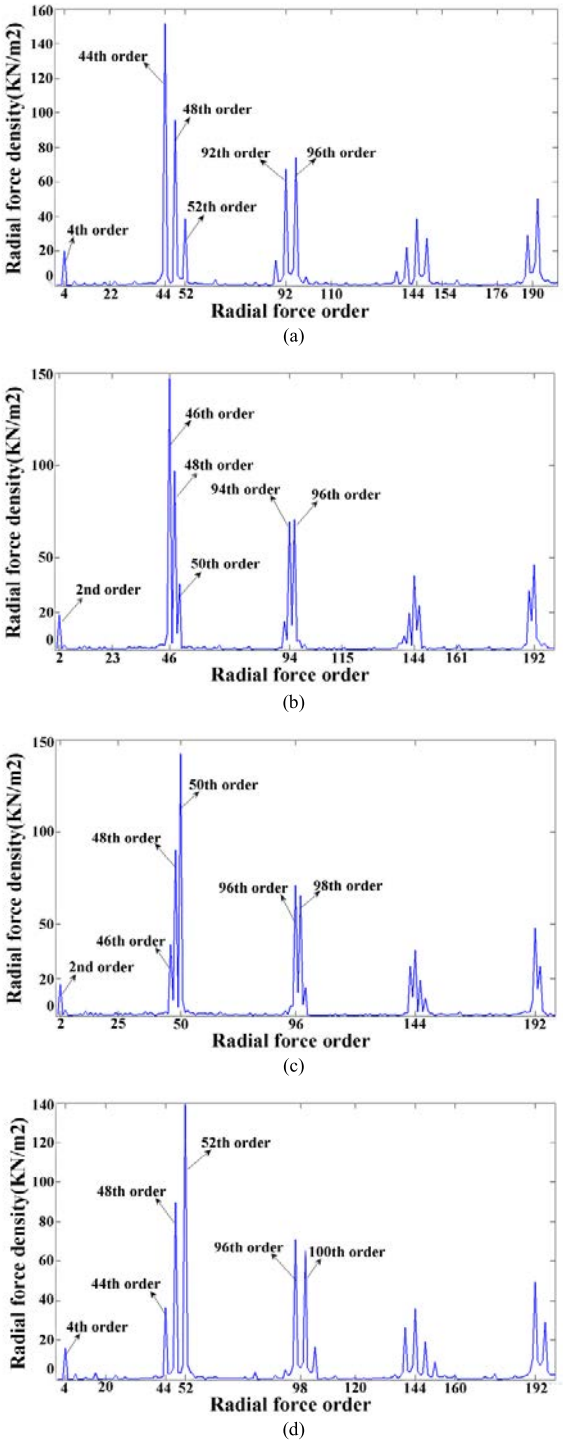

FIGURE 5. Radial electromagnetic force at rated load. (a) 48 slots/ 44 poles. (b) 48 slots/ 46 poles. (c) 48 slots/ 50 poles. (d) 48 slots/ 52 poles.

When the order of radial electromagnetic force is equal or more than 2 ($\gamma \geq 2$), the core will be transformed. Considering bend and vibration, the natural frequency is:

$$f_\gamma = f_{\gamma 0} \frac{i\gamma\left(\gamma^2-1\right)}{\sqrt{\gamma^2+1}} \phi_\gamma \tag{7}$$

Where,

$$\phi_\gamma = \frac{1}{\sqrt{1+\dfrac{i^2\left(\gamma-1^2\right)\left[\gamma^2\left(4+\dfrac{\Delta_\gamma}{\Delta_0}\right)+3\right]}{\gamma^2+1}}}$$

$$i = \frac{1}{\sqrt{3}}\frac{h_e}{D_e}$$

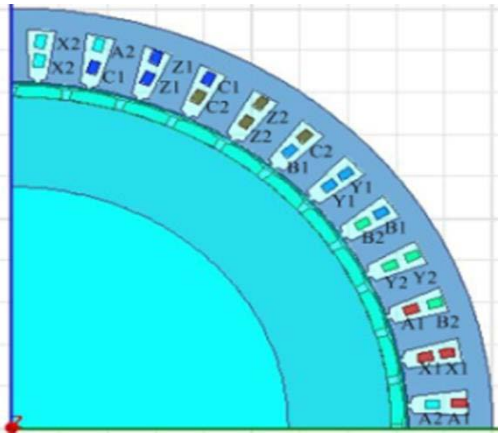

FIGURE 6. Winding arrangement of the motor prototype.

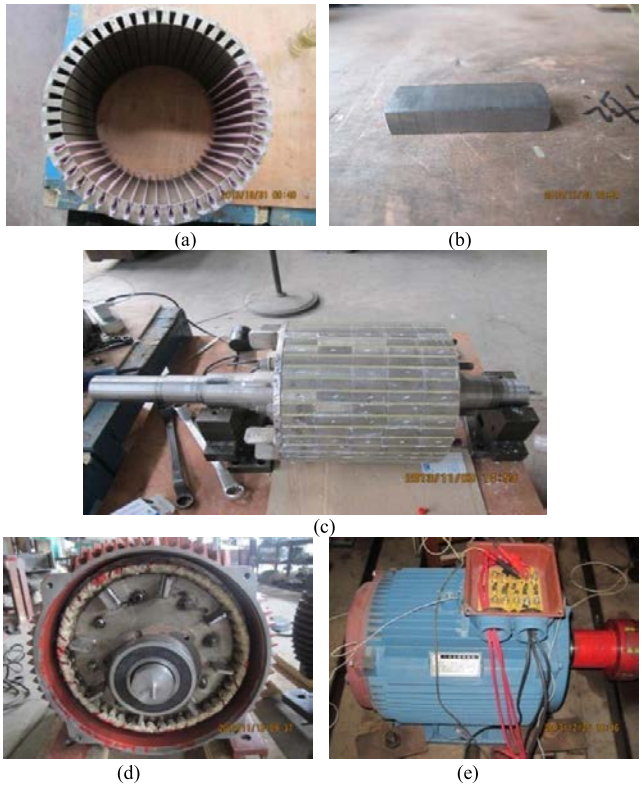

FIGURE 7. Structure of the prototype motor. (a) stator. (b) permanent magnet. (c) rotor. d) ending of motor. (e) whole motor.

When the frequency of core vibration caused by radial electromagnetic force equals or approaches natural frequency, resonance will happen. Meanwhile, deformation of core will be amplified, and the real deformation, namely displacement amplitude of core vibration is:

$$d = \frac{d_s}{\sqrt{\left[1 - \left(f/f_{\gamma 0}\right)^2\right]^2 + \left[\left(f/f_{\gamma 0}\right)\frac{c}{\pi}\right]^2}} \tag{8}$$

In equation (8), c is the damping coefficient.

From analysis above, motor vibration has direct ratio relationship with magnetic force and has inverse ratio relationship with the 3rd power of force order. When the motor vibration frequency equals or approaches to natural frequency, the vibration will be enhanced.

FIGURE 8. Experimental system.

FEM method is used to calculate the radial and tangential air-force flux density, and equation (2) is adopted to calculate radial electromagnetic force. Fig.5 and Table III show harmonic distribution of radial force at rated load.

To be convenient for discussion of harmonics in fractional-slot motor, the 2-pole wave, wave length of which equals to armature perimeter, is regarded as reference wave. As for this 2-pole wave, the generally spoken fundamental wave (corresponding to p pole pairs) becomes into p order wave, now called main wave in this paper. So the order of harmonic discussed in this paper equals to the pairs of poles.

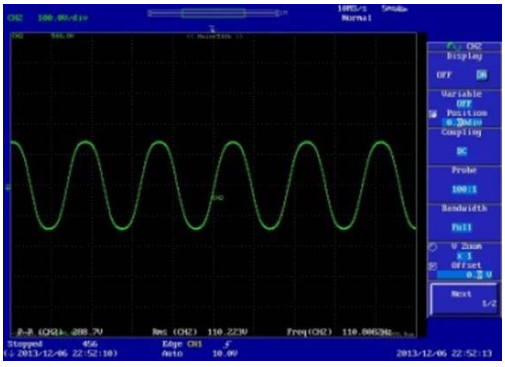

FIGURE 9. Phase EMF at Rated Motor Speed.

From the table above we can find that the 2nd order force appears in Case 2 and Case 3, but not in Case 1 and Case 4. It is known that lower order force will intensify the vibration. While comparing Case 1 and Case 4, lower order force is greater in the latter case. That means lower order radial force will be generated when the number of slot is close to that of poles, which will worsen the vibration characteristic.

Considering all the analysis above, the 48-slot 44-pole motor is the best scheme, and its vibration is the most satisfying.

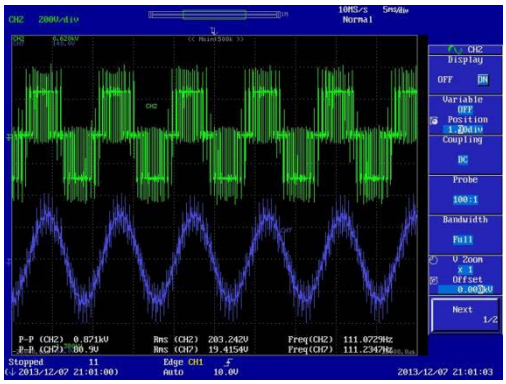

(a)

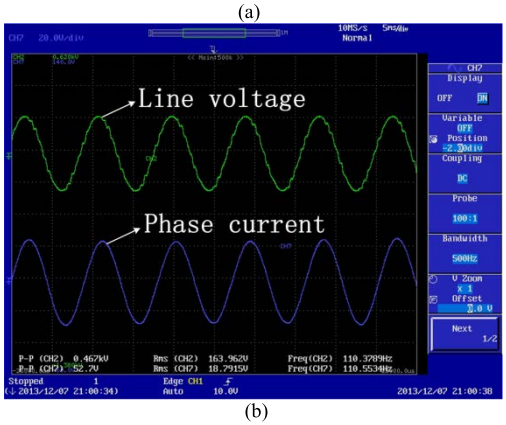

(b)

FIGURE 10. The waveforms of motor line voltage and phase current at rated load. (a) before filtering. (b) after filtering.

TABLE 4. Parameters of six-phase fractional-slot concentrated-winding permanent motor.

Parameters	Value	Parameters	Value
Rated power	20kW	Conductors per slot	32
Rated line voltage	380V	Rated torque	637 N.m
Pairs of poles	22	Rated phase current	17A
Slot number	48	Rated speed	300r/min
External diameter of stator	400mm	Eccentricity of poles	120mm
Inner diameter of stator	330mm	External diameter of rotor	327mm
Minimum air gap	1.5mm	Core length	255mm
Pole arc coefficient	0.83	Parallels	1
Winding serial turns of phase	128	Maximum height of permanent magnet	5.7mm

V. PROTOTYPE DESIGN AND EXPERIMENT

A. PROTOTYPE DESIGN AND MANUFACTURE

The scheme of 48-slot 44-pole motor is selected as the best one, and its final parameters are listed in Table IV.

Open slot and double-layer winding is adopted in the stator, and the permanent magnet material is N35UH. The type of silicon steel sheets used in both stator and rotor is 50DW310-Z. Ansoft software is used to simulate the motor. The winding arrangement is shown in Fig.6.

Prototype is manufactured according to the results of electromagnetic calculation, and the motor structure is shown in Fig.7. There are 5 permanent magnets on rotor in axial direction of each pole and each permanent magnet is divided into 10 small permanent magnets in order to decrease the influence of eddy current.

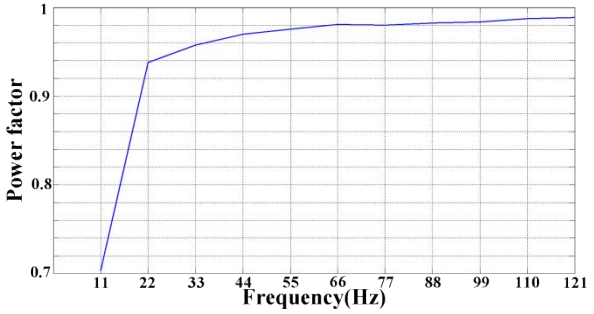

FIGURE 11. The curve of power factor varied with frequency under loaded status.

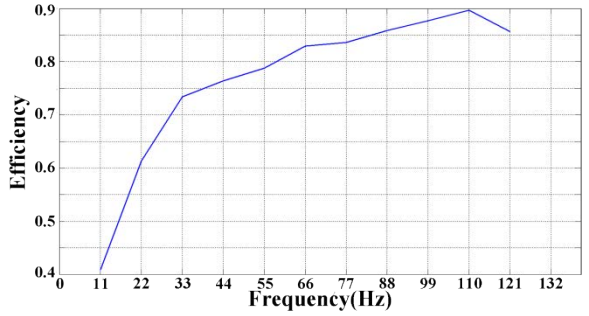

FIGURE 12. The curve of efficiency varied with frequency changed under loaded status.

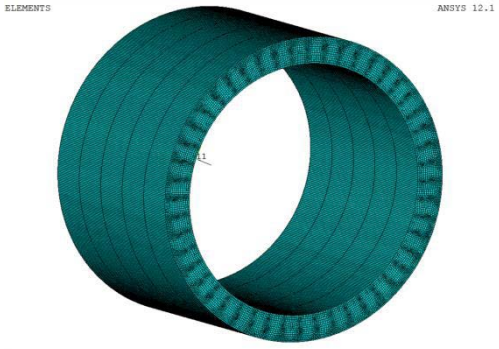

FIGURE 13. Grid of stator.

B. EXPERIMENT AND ANALYSIS

1) TEST OF ELECTROMAGNETIC PERFORMANCE

While doing the experiments, the motor is supplied by a six-phase inverter, and the load of motor is a six-phase PM motor. The test system is shown in Fig.8.

The designed motor is dragged to obtain its back EMF at different speeds. Fig.9 is the EMF at rated speed. Table V is comparison between measure and design EMF. The designed and tested results are in good agreement, and the error is less than 2%, which can meet with the engineering requirement.

When tested at rated load, the motor designed in this paper operates as an electromotor, directly dragging a

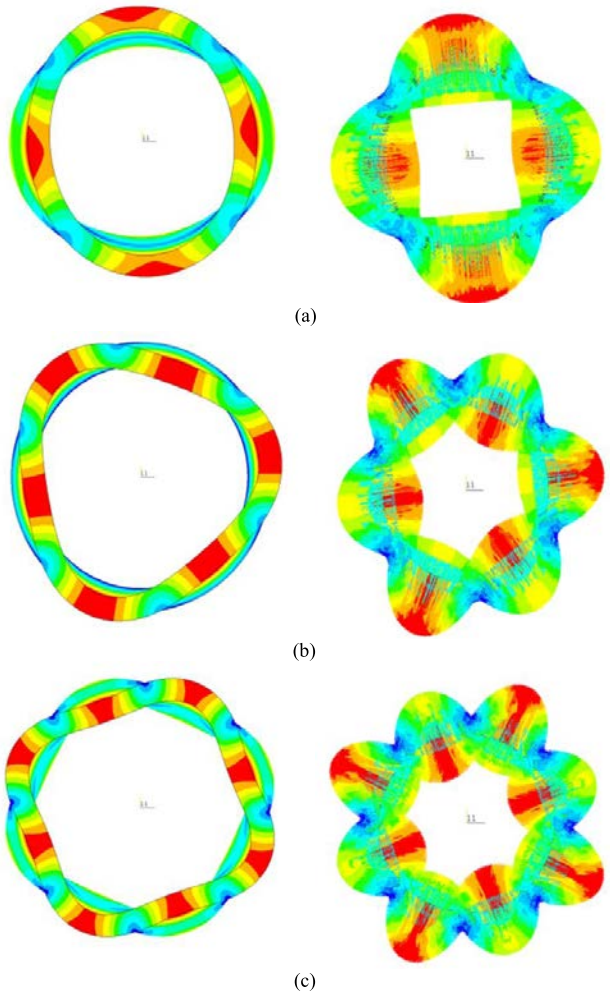

FIGURE 14. Vibration pattern and vector diagram of radial natural modal of stator. (a) 2nd order. (b) 3rd order. (c) 4th order.

TABLE 5. Motor phase back electromotive force comparison between measure value and design value.

	Amplitude of phase EMF	
	Fundamental wave	The 3rd harmonic
Test value（V）	308	29.2
Design value（V）	311	30
error	0.94%	1.45%

generator which can output rated power (20 kW) at rated speed (300r/min). Fig.10 (a) shows waveforms of phase current and line voltage at rated speed by direct measuring, and its filtered result is shown in Fig.10 (b).

The change of power factor with speed (frequency) is shown in Fig.11, from which we can see the motor power factor could be more than 0.94 when the frequency passes 22Hz (60r/min).

The change of efficiency following speed (frequency) is shown in Fig.12, from which we can see as speed rise up motor efficiency increases. And the efficiency reaches up to its maximum, namely 90%, when the speed is rated speed (300r/min,110Hz).

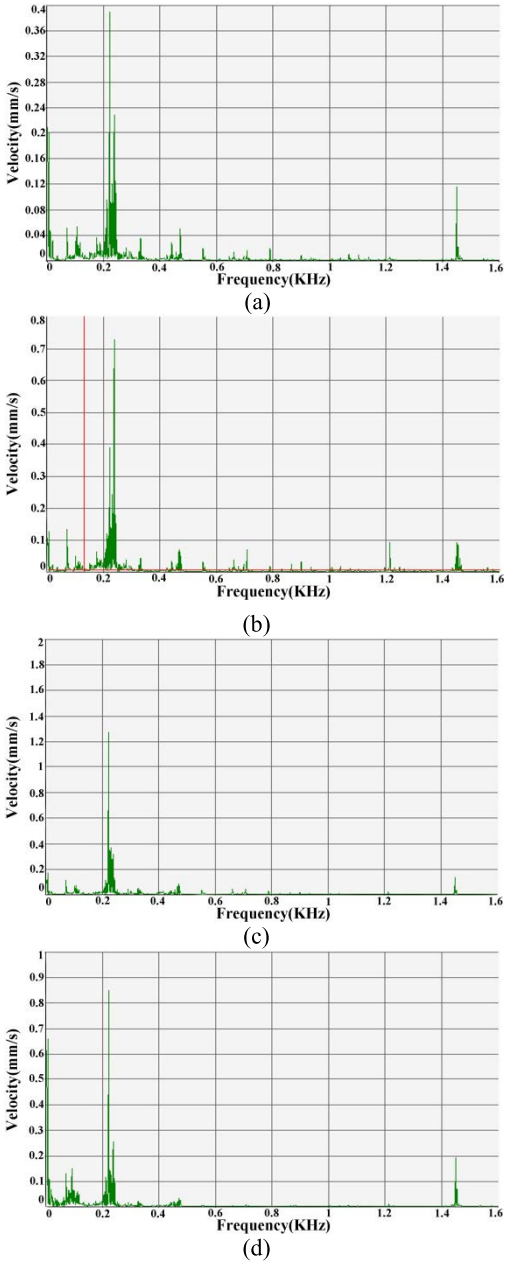

FIGURE 15. Acceleration distributions in frequency spectrum of motor under 300rpm. (a) test point of NO.1. (b) test point of NO.2. (c) test point of NO.3. (d) test point of NO.4.

From charts above, the motor designed in this paper has a good performance.

2) VIBRATION TEST

The Block Lanczos method of Ansys software is adopted to analyse the structural modal of motor. The modal steps of solution and extension are both 40. Not considering the influence of motor frame, 3-D modal FEM analysis of stator core and winding is conducted. Grid, vibration pattern and vector diagram of radial natural modal of stator are shown in Fig.13 and Fig.14. Natural frequencies corresponding to each vibration patterns are listed in Table VI.

TABLE 6. Natural frequency of stator.

Vibration pattern	Natural frequency of stator (Hz)
2nd order	408
3rd order	919
4th order	1449

Four test points are located on the motor, and acceleration sensor is placed at each test point. The NO.1 and NO.2 test points are located at the feet of motor, and NO.3 and NO.4 points are located at the top of motor. The inverter switching frequency is 2kHz. Acceleration of each point is tested at rated speed and load.

Tested accelerations of four points under different frequencies are listed in Fig.15, from which we can find that vibration acceleration reaches to its maximum under frequency that 2 times of input electrical frequency. The vibration of 1450 Hz (corresponding to 4th order force) is also relatively large, which is coincident with theory analysis in this paper.

VI. CONCLUSIONS

In this paper, we studied the six-phase fractional-slot concentrated-winding PM motor about its restraint conditions of slot-pole combination and method of optimizing selection. Air-gap flux density, radial electromagnetic force and harmonics of four motors are discussed. On the basis above, a 20kW prototype with 48 slots and 44 poles is designed and manufactured, and its electromagnetic and vibration characteristics are calculated and tested. Conclusions are as follows:

(1) Designing restraint conditions of six-phase semi-symmetrical fractional-slot concentrated-winding PM motor are discussed and its slot-pole combination schemes are obtained;

(2) The radial electromagnetic force of four types of motors (slot-pole combination schemes are 48/44, 48/46, 48/50 and 48/52) are calculated. The result indicated that lower order radial force will be generated when the number of slot is close to that of poles, which will worsen the vibration.

(3) With consideration of electromagnetic and vibration characteristics, a 20kW prototype of six-phase fractional-slot concentrated- winding PM motor with 48 slots and 44 poles is designed and manufactured. Its calculation and experiment results are in good agreement, which verifies the effectiveness of method proposed in this paper and the good performances of the motor designed. This paper has provided guidance for high-power propulsion motor applied in warships.

REFERENCES

[1] L. J. Wu, Z. Q. Zhu, J. T. Chen, Z. P. Xia, and G. W. Jewell, "Optimal split ratio in fractional-slot interior permanent magnet machines with non-overlapping windings," *IEEE Trans. Magn.*, vol. 46, no. 5, pp. 1235–1242, May 2010.

[2] M. Barcaro, A. Faggion, N. Bianchi, S. Bolognani, "Sensorless rotor position detection capability of a dual three-phase fractional-slot IPM machine," *IEEE Trans. Ind. Appl.*, vol. 48, no. 6, pp. 2068–2078, Nov./Dec. 2012.

[3] H. Yang and Y. Chen, "Influence of radial force harmonics with low mode number on electromagnetic vibration of PMSM," *IEEE Trans. Energy Convers.*, vol. 29, no. 1, pp. 38–45, Mar. 2014.

[4] Y. Li, S. Li, J. Xia, and F. Zhang, "Noise and vibration characteristics analysis on different structure parameters of permanent magnet synchronous motor," in *Proc. Int. Conf. Elect. Mach. Syst.*, Oct. 2013, pp. 46–49.

[5] L. Alberti and N. Bianchi, "Theory and design of fractional-slot multilayer windings," *IEEE Trans. Ind. Appl.*, vol. 49, no. 2, pp. 841–849, Mar./Apr. 2013.

[6] R. Dutta, L. Chong, and M. F. Rahman, "Design and experimental verification of an 18-Slot/14-pole fractional-slot concentrated winding interior permanent magnet machine," *IEEE Trans. Energy Convers.*, vol. 28, no. 1, pp. 181–190, Mar. 2013.

[7] T. Cox and J. F. Eastham, "Multi layer planar concentrated windings," in *Proc. Int. Elect. Mach. Drives Conf.*, Niagara Falls, ON, Canada, May 2011, pp. 1461–1466.

[8] S.-K. Lee, G.-H. Kang, and J. Hur, "Finite element computation of magnetic vibration sources in 100 kW two fractional-slot interior permanent magnet machines for ship," *IEEE Trans. Magn.*, vol. 48, no. 2, pp. 867–870, Feb. 2012.

[9] M. V. Cistelecan, F. J. T. E. Ferreira, and M. Popescu, "Three phase tooth-concentrated interspersed windings with low space harmonic content," in *Proc. 19th Int. Conf. Elect. Mach.*, Sep. 2010, pp. 1–6.

[10] L. Hao, "Design and analysis of IPM machine with bar wound fractional slot distributed winding for automotive traction application," in *Proc. Energy Convers. Congr. Expo. (ECCE)*, Sep. 2013, p. 598- 605.

MINGZHONG QIAO was born in Jiangsu, China, in 1971. He received the B.S. and Ph.D. degrees in electrical engineering from the Naval University of Engineering, Wuhan, China, in 1996 and 2003, respectively.

He is currently a Professor with the Department of Electrical Engineering, Naval University of Engineering. His current research interests include power system automation and ship propulsion motor.

CHAO JIANG was born in Hubei, China, in 1990. He received the B.S. degree in marine engineering from the Wuhan University of Technology, Wuhan, China, in 2013. He is currently pursuing the Ph.D. degree in electrical engineering with the Naval University of Engineering, Wuhan.

His current research interests include power system automation and ship propulsion motor.

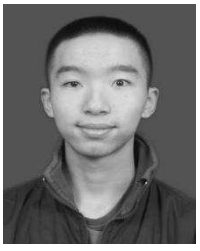

YONGXIN ZHU was born in Jiangsu, China, in 1992. He received the B.S. degree in computer science from Jilin University, Jilin, China, in 2014. He is currently pursuing the Ph.D. degree in electrical engineering with the Naval University of Engineering, Wuhan, China.

His current research interests include power system automation and ship propulsion motor.

GENG LI was born in Hubei, China, in 1987. He received the B.S. degree in automation from Wuhan Polytechnic University, Hubei, in 2010. He is currently pursuing the Ph.D. degree in electrical engineering with the Naval University of Engineering, Wuhan, China.

His current research interests include power system automation and ship propulsion motor.